https://doi.org/10.56801/MME1048

Increasing Surface Hardness and Corrosion Resistance of AISI 410 Stainless Steel by Forming a Diamond-Like Carbon Thin Film

Agung Setyo Darmawan[1], Agus Yulianto[1], Bambang Waluyo Febriantoko[1], Bibit Sugito[1], Suprapto[2], Tjipto Sujitno[2], Turnad Lenggo Ginta[3], Abdul Hamid[4]

[1]*Mechanical Engineering Department, Universitas Muhammadiyah Surakarta, Indonesia*
[2]*Center for Accelerator Technology and Materials Process, National Research and Innovation Agency (BRIN), Indonesia*
[3]*Research Center for Manufacture and Industrial Process Technology, National Research and Innovation Agency (BRIN), Indonesia*
[4]*Technology Education Department, Universiti Tun Hussein Onn Malaysia, Malaysia*

Received: 13-01-2024; Revised: 09-02-2024
Accepted: 13-02-2024; Published: 07-03-2024

Abstract: AISI 410 stainless steel plays an important role in many engineering fields. The annealing process of this material will increase toughness. But this process will also reduce the hardness of the material. Plasma chemical vapor deposition was carried out to increase the surface hardness and corrosion resistance of AISI 410 stainless steel. In this study, the raw material was tested for metallography, hardness, and corrosion resistance. Then an annealing process was carried out on the raw material. The annealed material was also observed for metallography, hardness, and corrosion resistance. Furthermore, on the annealed material, the plasma chemical vapor deposition process was carried out with pressure variations of 1.0, 1.2, 1.4, and 1.6 mbar. Next, the material was tested for metallography with a scanning electron microscope to measure the layer thickness. The formation of diamond-like carbon was confirmed by the Raman Spectroscopy test. Annealed followed by plasma chemical vapor deposition processed AISI 410 stainless steel also tested for hardness and corrosion. The results showed that the annealed AISI 410 stainless steel underwent a phase change from martensite and retained austenite to ferrite and pearlite. The annealed raw material experienced a decrease in hardness and corrosion rate. After the annealed material was processed by plasma chemical vapor deposition, The thickness of the surface layer increased with increasing pressure. Along with that, the hardness and corrosion resistance increased.

Keywords: AISI 410; Corrosion: Hardness; PCVD.

1. Introduction

AISI 410 stainless steel material has various applications in engineering fields such as screws, valves, shafts, bearings, and blades in compressors and turbines [1-3]. This material has good strength, corrosion resistance, and wear resistance [4-6]. However, due to its application to components with high strains, it results in fatigue failure due to local plastic deformation [7].

Heat treatment is needed to produce effective mechanical properties in preventing large plastic deformation. It is a process that involves heating and cooling metals in a solid state for a set time to achieve specific qualities. Heating and cooling can both produce changes in the metal phase. This structural alteration changes the properties [8-10].

Annealing is one of the heat treatment methods. Annealing is a heat treatment method that involves heating the metal to a specific temperature, keeping it at that temperature for a specific amount of time to achieve the desired alteration, and then cooling the metal at a relatively slow cooling rate. Annealing can be performed on workpieces under various conditions and for various purposes. Annealing can increase softness, ductility, and toughness, and produce certain microstructures [11, 12].

Apart from heat treatment, surface treatment to form a film is needed to improve the surface properties of the material due to failures such as fatigue, wear, and corrosion which originate directly from the material's surface. One type of surface treatment is plasma chemical vapor deposition (PCVD). PCVD can be done to form a layer containing diamond-like carbon (DLC) [13]. DLC coatings exist in several different forms of amorphous carbon materials that display some of the unique properties of diamonds. This method produces excellent material properties such as high hardness [14], low friction coefficient [15], increased wear [16], and corrosion resistance under extreme working conditions [17].

DLC coatings can be amorphous, more or less flexible, hard, and high strength, according to the composition and processing method. Film formation can be obtained by plasma chemical vapor deposition [18, 19], ion beam deposition [20, 21], sputtering [22, 23], and RF plasma deposition [24, 25].

DLC films belong to the group of amorphous carbon-based materials, which possess many unique properties and have been widely studied due to their potential applications in medicine [26-28], industry [29-31], electrochemistry [32, 33], micro and optoelectronics [34-36]. High-quality DLC films with high sp^3 fraction content have properties similar to diamond, while films with lower sp^3 content exhibit properties similar to graphite and other carbon materials that have sp^2 bonding configuration [37, 38].

The formation of a DLC layer on a metal surface using the PCVD method usually uses a mixture of hydrocarbon gas and argon (Ar). Some of the most widely used hydrocarbon gases include methane (CH_4), ethane (C_2H_6), propane (C_3H_8), butane (C_4H_{10}), and benzene (C_6H_6). These materials are expensive. Hydrocarbon materials can be replaced using other materials such as Liquified Petroleum Gas (LPG). 97.5% of LPG gas is a mixture of propane (C_3H_8) and butane (C_4H_{10}), and the rest is hydrocarbons such as ethane (C_2H_6) and pentane (C_5H_{12}) and other impurities at very low levels. LPG gas has a cheaper price and is easily available on the market [39].

Hardness plays an important role when materials are used as friction components [40-44]. Meanwhile, in service, the material may experience corrosion phenomena which will reduce its mechanical properties [45]. Therefore, this research is aimed at increasing the surface hardness and decreasing the corrosion rate of annealed AISI 410 steels.

2. Material and Methods

The material used in this research was AISI 410 stainless steel. AISI 410 stainless steel is martensitic stainless steel. The composition of these stainless steels is shown in Table 1.

Table 1. *The chemical composition of AISI 410 Stainless Steel*

Element	C	Si	Mn	P	S	Ni	Cr
Weight %	0.1-0.15	0.8	1.00	0.03	0.035	0.06	12-13

To achieve the specified objectives, this research was carried out in 3 stages. The first stage was research on raw material AISI 410 stainless steels, the second stage was research on annealed AISI 410 stainless steels, and the last stage was research on the PCVD of annealed AISI 410 stainless steels to form a thin layer of DLC.

In the first stage, a metallographic observation was carried out with a RaxVision MM10A optical microscope to determine the microstructure of AISI 410 stainless steels. Hardness testing was carried out using Hirox brand micro-Vickers equipment with serial number FMS8135 to determine the raw material's hardness. The load used in this hardness test was 10 gf with an indentation time of 10 seconds. Then, electrochemical corrosion resistance testing was carried out using a Parstat brand potentiostat.

The second stage was carried out by annealing AISI 410 stainless steels at 900^{o}C, holding for 20 minutes, and cooling in the furnace to room temperature (Figure 1). Furthermore, metallographic examination was carried out with an optical microscope, hardness testing with the micro-Vickers technique, and electrochemical corrosion resistance testing with a potentiostat.

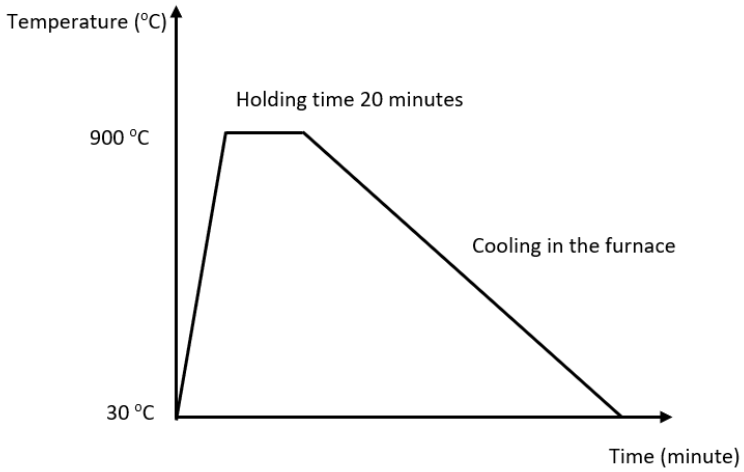

Figure 1. *Annealing Process Schematic*

The third stage is the process of the PCVD technique on annealed AISI 410 stainless steels. PCVD was carried out with pressure variations of 1.0, 1.2, 1.4, and 1.6 mbar. Then metallographic examination was carried out using a Scanning Electron Microscope (SEM) brand Thermo-Scientific type Phenom Pro X to observe the thickness of the DLC layer formed, hardness testing with the micro-Vickers technique, and electrochemical corrosion resistance testing with a potentiostat. Next, the specimen annealed and PCVD-processed with a pressure of 1.0 mbar was examined using Raman spectroscopy to confirm the formation of DLC. In this research, Raman Spectroscopy was tested using the RAMAN HORIBA iHR320. The test was carried out with a laser excitation wavelength of 532 nm in the Raman shift range of 200 – 3000 cm^{-1}.

3. Material and Methods

3.1 Metallographic Testing of AISI 410 Stainless Steels

Figure 2 shows the microstructure of AISI 410 stainless steel raw material produced with an optical microscope. In the microstructure, it can be analyzed that the raw material had martensite and retained austenite phases. The martensite phase appeared as alternating black and white needles. While the retained austenite phase appeared in the form of white grains [46].

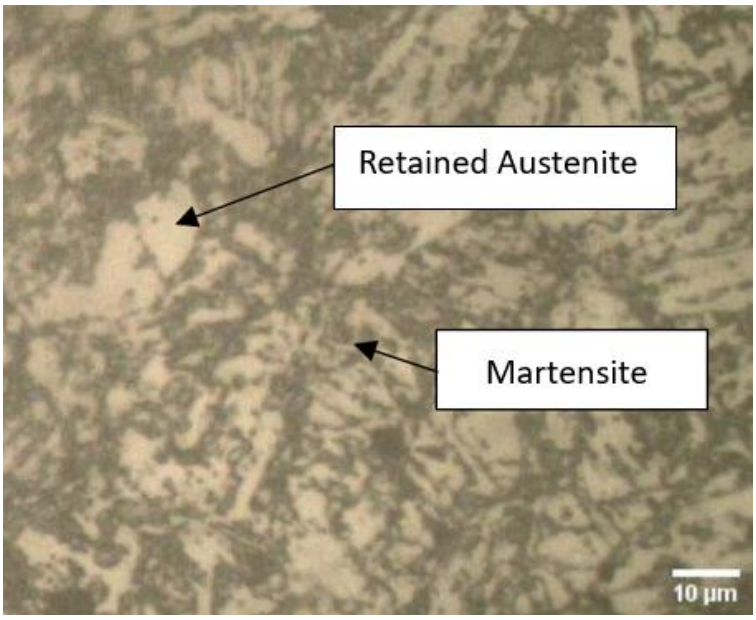

Figure 2. *Microstructure of raw material AISI 410 stainless steels*

Process annealing was conducted on raw material AISI 410 stainless steel to reduce the brittleness and increase the ductility. The microstructure was observed using an optical microscope. Figure 3 shows the phases that appeared in annealed AISI 410 stainless steels. In the figure, there were ferrite and pearlite phases. The visible ferrite phase was white. Meanwhile, the pearlite phase appeared in alternating light and dark lamellar forms. Slow cooling in the furnace caused the carbon atoms to diffuse out of the face center cubic (FCC) unit cell so that the austenite transformed into pearlite instead of martensite [47].

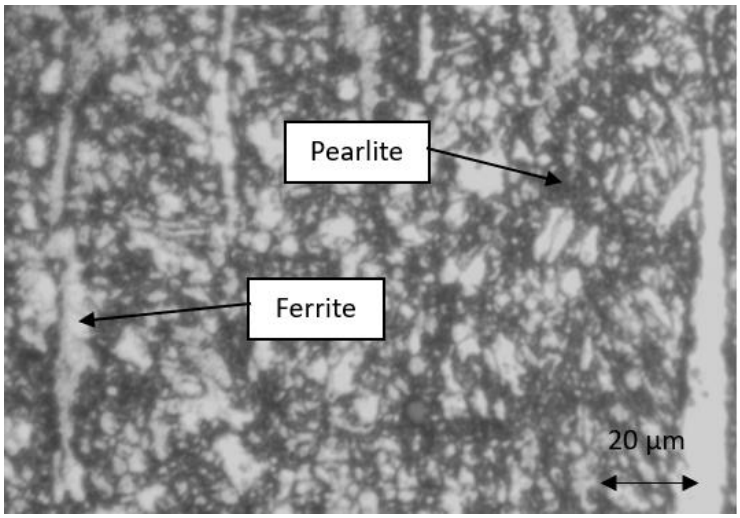

Figure 3. *Microstructure of annealed AISI 410 stainless steels*

Next, the PCVD process was carried out on annealed AISI 410 stainless steels. This process formed a DLC thin film on the surface of annealed AISI 410 stainless steels. The PCVD process was carried out with pressure variations of 1.0, 1.2, 1.4, and 1.6 mbar. The thickness of the thin film was observed by SEM and is shown in Figure 4.

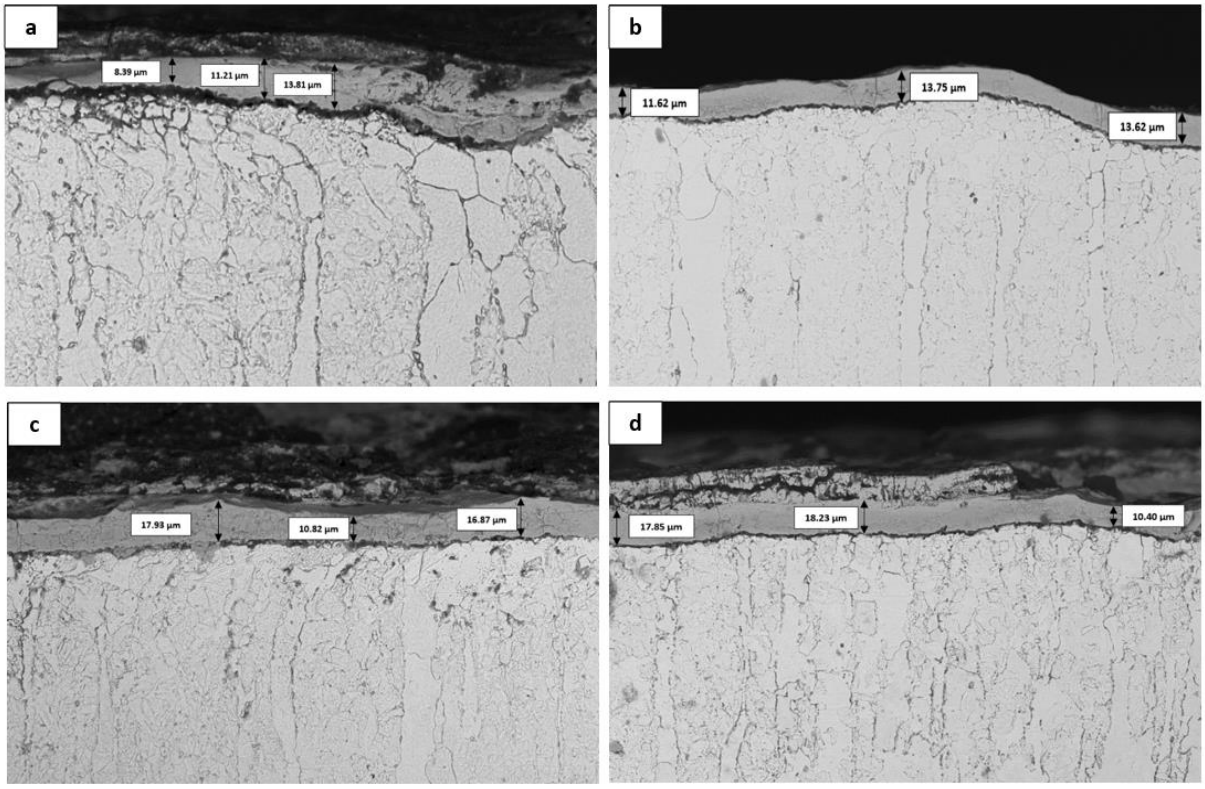

Figure 4. *The DLC thin film thickness of annealed followed by PCVD-processed AISI 410 stainless steels at a pressure of (a) 1.0 mbar (b) 1.2 mbar (c) 1.4 mbar (d) 1.6 mbar*

The effect of pressure variations on DLC thin film thickness is shown in Figure 5. The PCVD process with pressure variations of 1.0, 1.2, 1.4, and 1.6 mbar produces average layer thicknesses of 11.4, 13.0, 15.21, and 15.49 µm, respectively. From a pressure of 1.0 to a pressure of 1.6 mbar there is an increase in thickness of 39%.

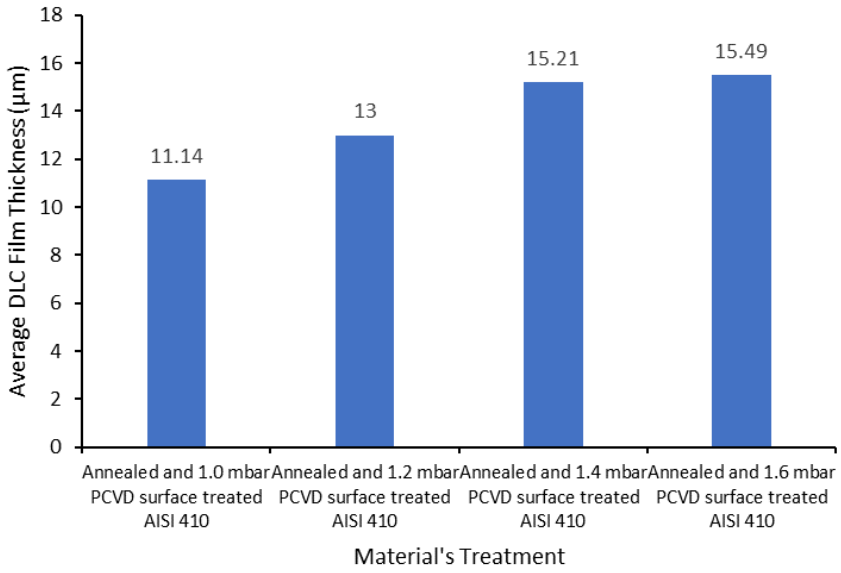

Figure 5. *PCVD pressure variations effect of annealed AISI 410 stainless steels on DLC thin film thickness*

Energy Dispersive Spectroscopy (EDS) testing was carried out to determine the elemental composition of the thin layer on the surface of annealed and PCVD-processed AISI

410 stainless steels with a pressure of 1.0 mbar. EDS testing on a thin layer of AISI 410 stainless steel (Figure 6a) produced an EDS line analysis as in Figure 6b which shows the appearance of several elements that made up the thin layer of AISI 410 steel. In the thin layer, there are carbon (C) elements of 12.249 wt%, oxygen (O) of 25.301 wt%, chromium (Cr) of 17.972 wt%, and iron (Fe) of 44.478 wt%. Carbon elements were formed in this layer, but it cannot be determined whether it is DLC or not. The certainty of the appearance of the DLC layer will be confirmed with a Raman Spectroscopy test.

Furthermore, EDS testing on the boundary between the thin layer and the AISI 410 steel substrate (Figure 7a) produced EDS line analysis as in Figure 7b which shows several elements that made up the boundary between the thin layer and the substrate. At this boundary, the element carbon (C) appears at 52.314 wt%, oxygen (O) at 19.014 wt%, sodium (Na) at 1.710 wt%, aluminum (Al) at 0.604 wt%, chlorine (Cl) of 1.408 wt%, potassium (K) of 0.905 wt%, titanium (Ti) of 1.207 wt%, chromium (Cr) of 5.835 wt%, iron (Fe) of 17.002 wt%. The carbon content at the boundary between the thin layer and the substrate shows a higher value than the carbon content in the thin layer.

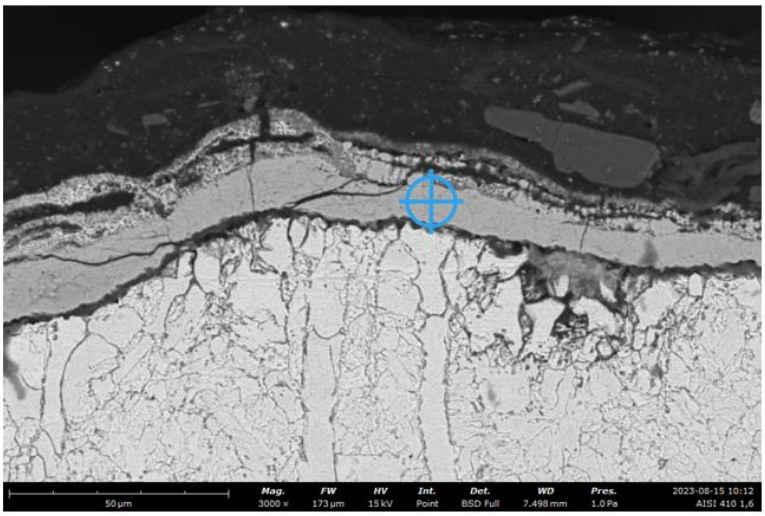

(a)

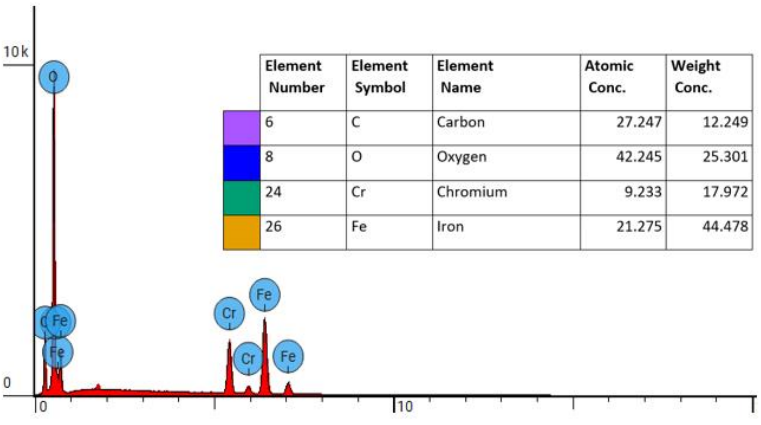

Element Number	Element Symbol	Element Name	Atomic Conc.	Weight Conc.
6	C	Carbon	27.247	12.249
8	O	Oxygen	42.245	25.301
24	Cr	Chromium	9.233	17.972
26	Fe	Iron	21.275	44.478

(b)

Figure 6. *EDS testing on a thin layer of AISI 410 steel (a) location (b) composition analysis*

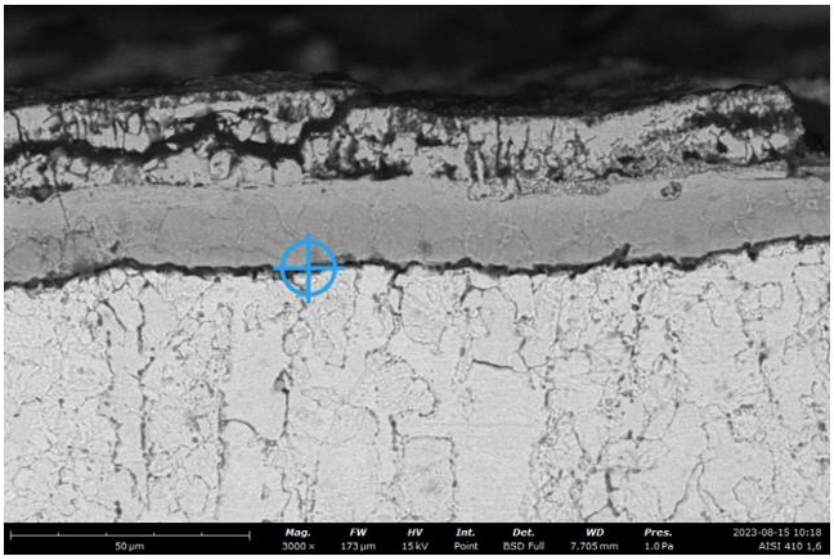

(a)

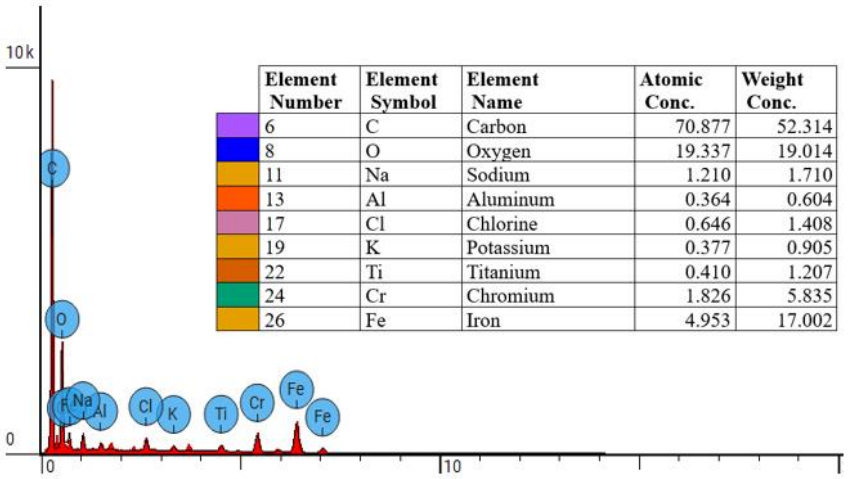

Element Number	Element Symbol	Element Name	Atomic Conc.	Weight Conc.
6	C	Carbon	70.877	52.314
8	O	Oxygen	19.337	19.014
11	Na	Sodium	1.210	1.710
13	Al	Aluminum	0.364	0.604
17	Cl	Chlorine	0.646	1.408
19	K	Potassium	0.377	0.905
22	Ti	Titanium	0.410	1.207
24	Cr	Chromium	1.826	5.835
26	Fe	Iron	4.953	17.002

(b)

Figure 7. *EDS testing on a boundary between thin layer and substrate of AISI 410 steel (a) location (b) composition analysis*

3.2 Raman Spectroscopy Testing of AISI 410 Stainless Steels Thin Film

Raman Spectroscopy testing aimed to confirm the presence of a DLC layer on the surface of the material. The D peak and G peak can be identified to determine qualitatively the structure of the sp^3 (diamond) and sp^2 (graphite) content in the DLC layer [48]. The test results were in the form of a spectrum image which can be seen in Figure 8.

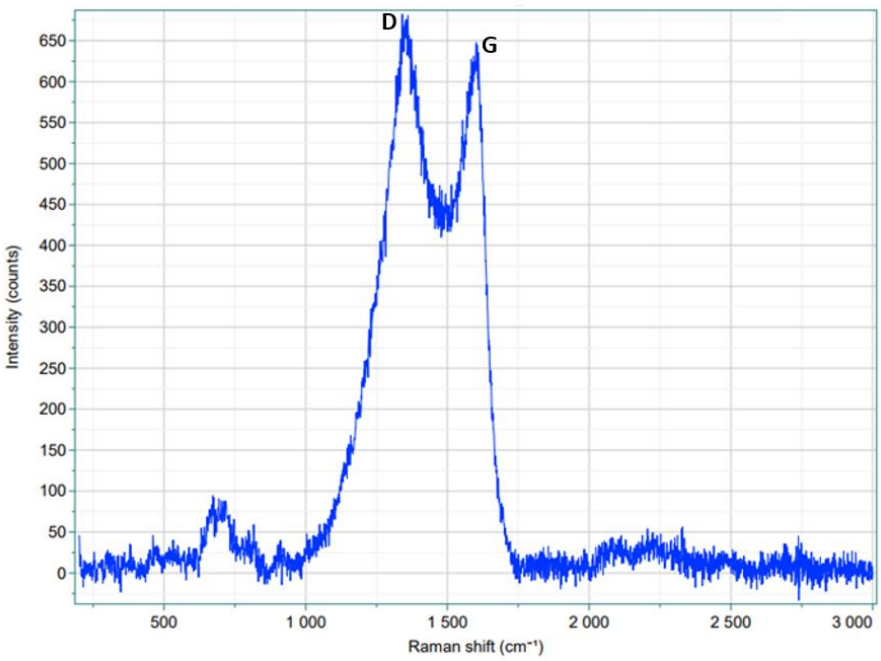

Figure 8. *Raman Spectroscopy Test Results for Annealed and PCVD-processed AISI 410 Stainless Steel*

Based on the results of Raman Spectroscopy testing on AISI 410 stainless steel which was annealed and followed by PCVD with a pressure of 1.6 mbar, the D peak (sp^3) was obtained at a Raman shift of 1360.44 cm^{-1} with an intensity of 680.882 counts, and the G peak (sp^2) was obtained at a Raman shift of 1604. 94 cm^{-1} with an intensity of 644.689 counts. The D Peak was in the shift range of around 1350 cm^{-1} while the G peak was in the shift range of around 1580 – 1600 cm^{-1}. Thus, it was shown that a DLC layer was formed [49].

3.3 Hardness Testing of AISI 410 Stainless Steels

The hardness test results are shown in Figure 9. Hardness test results on raw material AISI 410 stainless steels, annealed AISI 410 stainless steels, annealed and PCVD-processed AISI 410 stainless steels with the pressure of 1.0, 1.2, 1.4, and 1.6 mbar were 289.49, 242.45, 299.45, 322.14, 373.04, and 575.68 VHN, respectively. A decrease in hardness occurred when the raw material was annealed. Hardness decreased 16% from 289.49 VHN to 242.45 VHN. Phase transformation of martensite and retained austenite (Figure 2) to pearlite and ferrite (Figure 3) reduced the hardness level. The hardness of AISI 410 stainless steel which was annealed following the PCVD process showed a higher level of hardness than raw material and annealed AISI 410 stainless steel. This was caused by the formation of a thin layer of DLC (Figure 4). From a pressure of 1.0 to a pressure of 1.6 mbar, there was an increase in hardness of 92%. Surface hardness increased with increasing pressure, this was because the DLC thin film on the surface became thicker and porosity decreased [50].

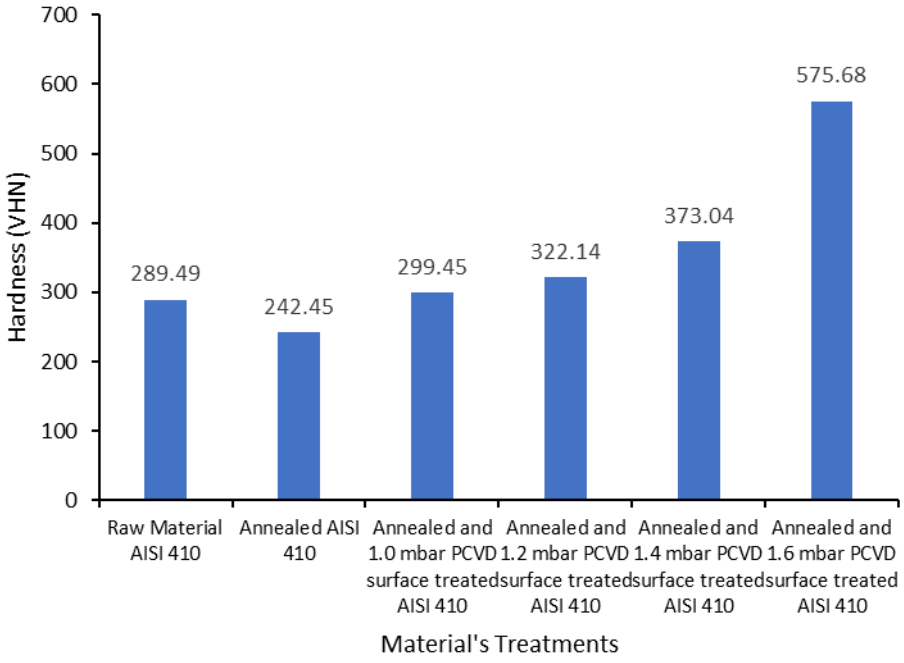

Figure 9. *PCVD pressure variations effect of annealed AISI 410 stainless steels on the hardness*

3.4 Corrosion Testing of AISI 410 Stainless Steels

The result of corrosion testing on the raw material AISI 410 stainless steel specimen is shown in Figure 10a. The figure shows that the I_{corr} value was 9.5736E-05 A/cm^2. The corrosion rate of the raw material AISI 410 stainless steel which had a mass of 5.99 g with a diameter of 14 mm and a height of 5 mm was 1.1231 mmpy.

Meanwhile, the results of corrosion testing on AISI 410 stainless steel specimens which were subjected to an annealing process at a temperature of 850^{o}C with a holding time of 20 minutes showed a Tafel curve as in Figure 10b. This curve shows that the I_{corr} value is 7.4277E-05 A/cm^2 which had a mass of the object 6.02 g with a diameter of 14 mm and a body height of 5 mm. Then the value of the corrosion rate was 0.87135 mmpy.

After carrying out the PCVD surface treatment process with a pressure of 1.0 mbar, an I_{corr} of 7.1817E-06 A/cm^2 was obtained and a corrosion rate of 0.08425 mmpy (Figure 10c), the PCVD surface treatment process with a pressure of 1.2 mbar, obtained an I_{corr} of 1.4167E-06 A/cm^2 and a corrosion rate of 0.01662 mmpy (Figure 10d), the PCVD surface treatment process with a pressure of 1.4 mbar, obtained I_{corr} 1.0648E-06 A/cm^2 and a corrosion rate of 0.012492 mmpy (Figure 10e), the PCVD surface treatment process with a pressure of 1.6 mbar, obtained an I_{corr} of 5.0269E-07 A/cm^2 and a corrosion rate of 0.005897 mmpy (Figure 10f).

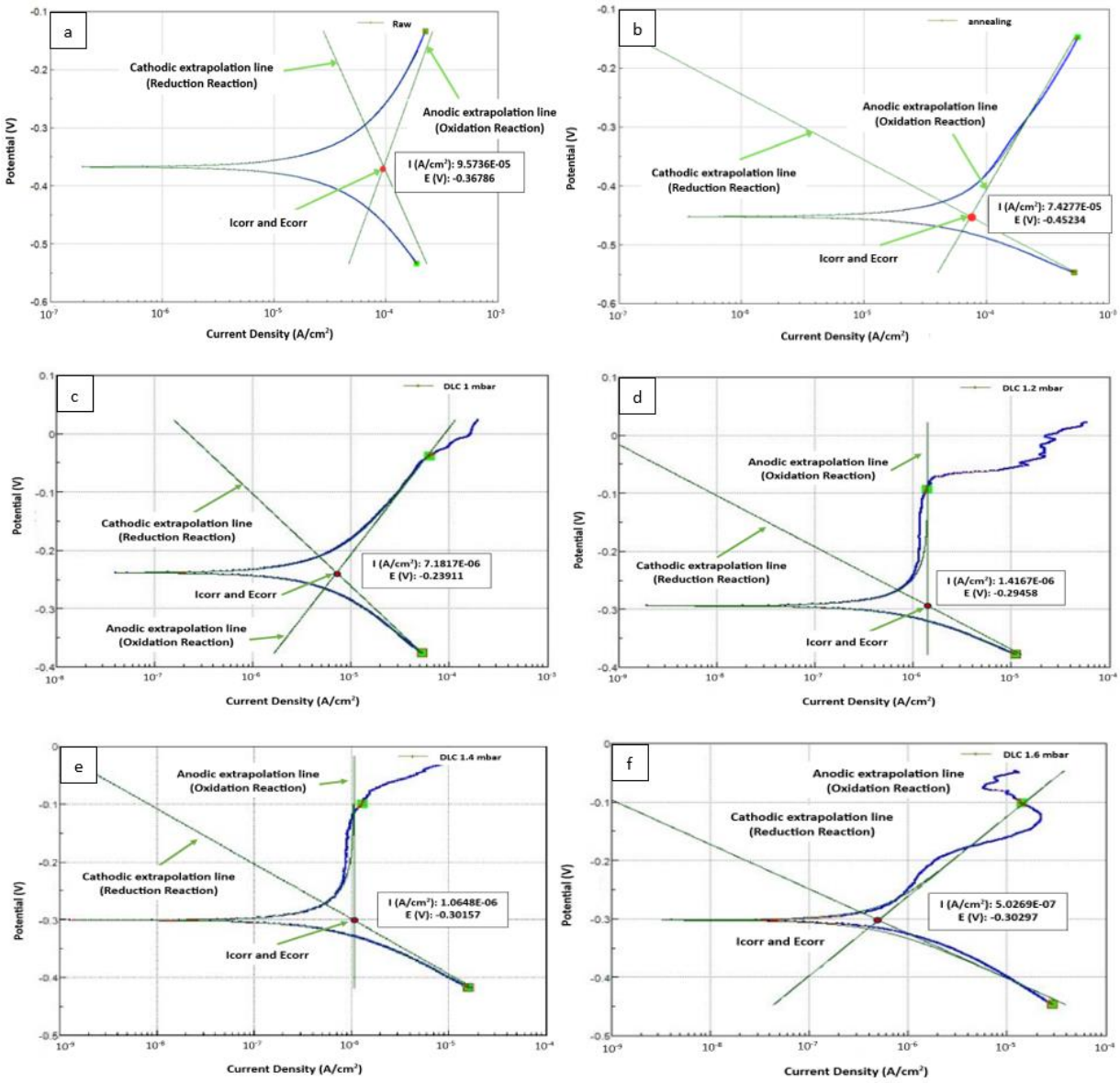

Figure 10. *Corrosion test results on (a) AISI 410 raw material, (b) Annealed AISI 410, (c) Annealed and 1.0 mbar PCVD surface treated AISI 410, (d) Annealed and 1.2 mbar PCVD surface treated AISI 410, (e) Annealed and 1.4 mbar PCVD surface treated AISI 410, (f) Annealed and 1.6 mbar PCVD surface treated AISI 410*

Figure 11 shows the effect of the annealing process and pressure variations of the PCVD process on the corrosion rate of AISI 410 Stainless Steel. The PCVD process showed a very significant influence. The presence of the DLC film reduced the corrosion rate of annealed AISI 410 stainless steels. This DLC film will protect the stainless steel from direct contact with the environment thereby inhibiting the ongoing corrosion process [51-53]. The thicker the layer containing DLC, the higher the corrosion resistance.

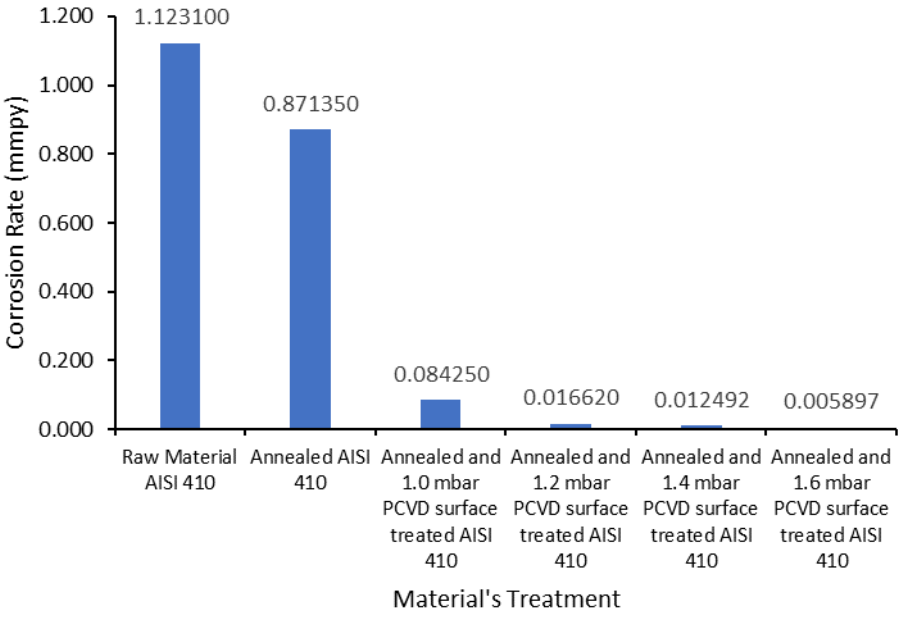

Figure 11. *The effect of the annealing process and pressure variations of the PCVD process on the corrosion rate of AISI 410 Stainless Steel*

4. Conclusion

The annealing process reduces the hardness and increases the corrosion resistance of AISI 410 stainless steel. The plasma chemical vapor deposition process increases the surface hardness and corrosion resistance of AISI 410 stainless steel. This process produces a thin layer of diamond-like carbon on the surface of AISI 410 stainless steel. The results of hardness and corrosion testing show that process pressure affects hardness and corrosion resistance. The higher the pressure, the harder and corrosion resistance increases.

Funding Details: This work was supported by the Education and Culture Ministry, Republic of Indonesia under Grant number 006 /LL6/PB/AL.04/2023, 170.3/C.1-III/LRI/VI/2023.

References

1. Zhang, Y., et al., *Damage and cracking prediction of AISI 410 martensitic stainless steel at elevated temperatures.* steel research international, 2021. **92**(9): p. 2100030.
2. Zhang, H., et al., *Assessment of the properties of AISI 410 martensitic stainless steel by an eddy current method.* Materials, 2019. **12**(8): p. 1290.
3. Moradi, M., H. Arabi, and M. Shamsborhan, *Multi-objective optimization of high power diode laser surface hardening process of AISI 410 by means of RSM and desirability approach.* Optik, 2020. **202**: p. 163619.
4. Moradi, M., et al., *A comparative study of laser surface hardening of AISI 410 and 420 martensitic stainless steels by using diode laser.* Optics & Laser Technology, 2019. **111**: p. 347-357.
5. Moreira, D., et al., *Failure analysis of AISI 410 stainless-steel piston rod in spillway floodgate.* Engineering Failure Analysis, 2019. **97**: p. 506-517.
6. George, P. and D.P. Selvaraj, *Cutting parameter optimization of CNC dry milling process of AISI 410 and 420 grade MSS.* Materials Today: Proceedings, 2021. **42**: p. 897-901.

7. Adinoyi, M.J., N. Merah, and J. Albinmousa, *Strain-controlled fatigue and fracture of AISI 410 stainless steel.* Engineering Failure Analysis, 2019. **106**: p. 104166.
8. Jahromi, S.J., A. Khajeh, and B. Mahmoudi, *Effect of different pre-heat treatment processes on the hardness of AISI 410 martensitic stainless steels surface-treated using pulsed neodymium-doped yttrium aluminum garnet laser.* Materials & Design, 2012. **34**: p. 857-862.
9. Xie, J., et al., *Effect of high-pressure heat treatment on the recrystallization and recrystallization texture of CC 5005 aluminum alloy.* Journal of Materials Research and Technology, 2023. **26**: p. 2017-2027.
10. Alagheband, M. and M. Ghanbari, *Experimental investigation on the effect of heat treatment parameters on the mechanical and microstructural properties of an ASTM A860 WPHY 65 pipe fitting.* Results in Materials, 2023. **19**: p. 100435.
11. Kainth, M., M. Singh, and A. Singh, *Effect of filler metal combination and post weld heat treatment on pitting corrosion and impact toughness of GTA welded AISI 410 SS joints.* Materials Today: Proceedings, 2022. **56**: p. 3035-3041.
12. Jin, B., et al., *Effect of annealing treatment on microstructural evolution and compressive behavior of Al0. 5CrFeNi2. 5Si0. 25 high-entropy alloy.* Materials Characterization, 2023. **205**: p. 113233.
13. Kovacı, H., et al., *Corrosion and tribocorrosion properties of duplex surface treatments consisting of plasma nitriding and DLC coating.* Tribology International, 2021. **156**: p. 106823.
14. Javidparvar, A.A., M.A. Mosavi, and B. Ramezanzadeh, *Nickel-aluminium bronze (NiBRAl) casting alloy tribological/corrosion resistance properties improvement via deposition of a Cu-doped diamond-like carbon (DLC) thin film; optimization of sputtering magnetron process conditions.* Materials Chemistry and Physics, 2023. **296**: p. 127279.
15. Polaki, S., et al., *Tribological properties of chemically modified diamond like carbon films in hydrogen plasma.* Tribology International, 2015. **81**: p. 283-290.
16. Rothammer, B., et al., *Evaluation of the wear-resistance of DLC-coated hard-on-soft pairings for biomedical applications.* Wear, 2023. **523**: p. 204728.
17. Wongpanya, P., et al., *Improvement in corrosion resistance of 316L stainless steel in simulated body fluid mixed with antiplatelet drugs by coating with Ti-doped DLC films for application in biomaterials.* Corrosion Science, 2022. **208**: p. 110611.
18. An, K., et al., *Two-step fabrication of thin film encapsulation using laser assisted chemical vapor deposition and laser assisted plasma enhanced chemical vapor deposition for long-lifetime organic light emitting diodes.* Organic Electronics, 2021. **91**: p. 106078.
19. Kim, K.H., et al., *Silicon nitride deposited by laser assisted plasma enhanced chemical vapor deposition for next generation organic electronic devices.* Applied Surface Science, 2021. **541**: p. 148313.
20. Gier, C., et al., *Controlling the optical properties of hafnium dioxide thin films deposited with electron cyclotron resonance ion beam deposition.* Thin Solid Films, 2023. **771**: p. 139781.
21. Chen, H.-C., Y.-R. Lu, and S.-B. Chen, *Anisotropic stress mechanisms for different dielectric multi-layer films deposited by ion-beam assisted deposition on flexible substrates.* Thin Solid Films, 2023. **782**: p. 140026.
22. Depla, D., *On the role of chemisorption in the formation of the target surface compound layer during reactive magnetron sputtering.* Vacuum, 2023. **217**: p. 112391.
23. Ueshima, Y., et al., *Nanocrystalline Ag–Cu–Al Alloy thin films with densely dispersed alumina particles prepared using reactive sputtering method with Ar–O2 mixed gas.* Materialia, 2023. **30**: p. 101853.

24. Liu, X., et al., *Epitaxial CuO thin films prepared on MgAl2O4 (110) by RF-plasma assisted pulsed laser deposition.* Vacuum, 2019. **169**: p. 108932.
25. Tzeng, S.-S., et al., *Surface characterization and nanomechanical properties of diamond-like carbon films synthesized by RF plasma enhanced chemical vapor deposition.* Thin Solid Films, 2011. **519**(15): p. 4870-4873.
26. Rothammer, B., et al., *Amorphous carbon coatings for total knee replacements—part i: deposition, Cytocompatibility, chemical and mechanical properties.* Polymers, 2021. **13**(12): p. 1952.
27. Wang, H., L. Wang, and X. Wang, *Structure characterization and antibacterial properties of Ag-DLC films fabricated by dual-targets HiPIMS.* Surface and Coatings Technology, 2021. **410**: p. 126967.
28. Jastrzębski, K., et al., *Induced Biological Response in Contact with Ag-and Cu-Doped Carbon Coatings for Potential Orthopedic Applications.* Materials, 2021. **14**(8): p. 1861.
29. Zia, A.W. and M. Birkett, *Deposition of diamond-like carbon coatings: Conventional to non-conventional approaches for emerging markets.* Ceramics International, 2021. **47**(20): p. 28075-28085.
30. Rajak, D.K., et al., *Diamond-like carbon (DLC) coatings: Classification, properties, and applications.* Applied Sciences, 2021. **11**(10): p. 4445.
31. Scendo, M. and K. Staszewska-Samson, *Effect of temperature on anti-corrosive properties of diamond-like carbon coating on S355 steel.* Materials, 2019. **12**(10): p. 1659.
32. Li, Z., et al., *In situ chemical lithiation transforms diamond-like carbon into an ultrastrong ion conductor for dendrite-free lithium-metal anodes.* Advanced Materials, 2021. **33**(37): p. 2100793.
33. Dong, H., et al., *Study on conductivity and corrosion resistance of N-doped and Cr/N co-doped DLC films on bipolar plates for PEMFC.* Diamond and Related Materials, 2020. **110**: p. 108156.
34. Kurt, M.Ş., et al., *Influence of thickness of the sputtered diamond-like carbon (DLC) on electronic and dielectric parameters of the Au/DLC/n-Si heterojunction.* Journal of Materials Science: Materials in Electronics, 2021. **32**: p. 25214-25224.
35. Dwivedi, N., et al., *Correlation of sp3 and sp2 fraction of carbon with electrical, optical and nano-mechanical properties of argon-diluted diamond-like carbon films.* Applied surface science, 2011. **257**(15): p. 6804-6810.
36. Smietana, M., et al., *Application of diamond-like carbon films in optical fibre sensors based on long-period gratings.* Diamond and Related Materials, 2007. **16**(4-7): p. 1374-1377.
37. Robertson, J., *Comparison of diamond-like carbon to diamond for applications.* physica status solidi (a), 2008. **205**(9): p. 2233-2244.
38. Robertson, J., *Diamond-like amorphous carbon.* Materials science and engineering: R: Reports, 2002. **37**(4-6): p. 129-281.
39. Suprapto, S., et al. *The formation of diamond like carbon on carbon steel using plasma of argon-liquified petrolium gas mixing*. in *AIP Conference Proceedings*. 2018. AIP Publishing.
40. Hariningsih, H., L. Lutiyatmi, and T. Daryanto, *Effects of heat treatment on microstructure and hardness of D2 tools.* Applied Research and Smart Technology (ARSTech), 2022. **3**(1): p. 29-37.
41. Riyadi, T.W.B., *Mechanical properties of Cu surface in the laminated structure of Cr-Cu coatings.* Media Mesin: Majalah Teknik Mesin, 2017. **18**(1).

42. Purboputro, P., M. Hendrawan, and A. Hariyanto. *Use of bamboo fiber as a brake pad lining material and the influence of its portion on hardness and durability*. in *IOP conference series: materials science and engineering*. 2018. IOP Publishing.
43. Anggono, A.D., N. Kholis, and N. Ngafwan. *Structure and Mechanical Properties of Double Side Friction Stir Welded Aluminium AA6061 with the Addition of Cu Powder*. in *Materials Science Forum*. 2022. Trans Tech Publ.
44. Darmawan, A.S., W.A. Siswanto, and T. Sujitno, *Comparison of commercially pure titanium surface hardness improvement by plasma nitrocarburizing and ion implantation.* Advanced Materials Research, 2013. **789**: p. 347-351.
45. Darmawan, A.S., et al. *Effect of Increasing Salinity to Corrosion Resistance of 5052 Aluminum Alloy in Artificial Seawater*. in *Materials Science Forum*. 2019. Trans Tech Publ.
46. Sierra-Soraluce, A., et al., *Effect of microstructure on tensile properties of quenched and partitioned martensitic stainless steels.* Materials Science and Engineering: A, 2023. **864**: p. 144540.
47. Moradi, M., et al., *Nd: YAG laser hardening of AISI 410 stainless steel: Microstructural evaluation, mechanical properties, and corrosion behavior.* Journal of Alloys and Compounds, 2019. **795**: p. 213-222.
48. Bonu, V., et al., *Temperature dependent erosion and Raman analyses of arc-deposited H free thick DLC coating on Cr/CrN coated plasma nitrided steel.* Surface and Coatings Technology, 2022. **436**: p. 128308.
49. Jokari-Sheshdeh, M., F. Mahboubi, and K. Dehghani, *Structure and tribological behavior of diamond-like carbon coatings deposited on the martensitic stainless steel: The influence of gas composition and temperature.* Diamond and Related Materials, 2018. **81**: p. 77-88.
50. Girisha, K. and K.S. Rao, *Improvement of corrosion resistance of aisi 410 martensitic steel using plasma coating.* Materials Today: Proceedings, 2018. **5**(2): p. 7622-7627.
51. Darmawan, A.S., et al., *RESEARCH PAPER INCREASING HARDNESS AND CORROSION RESISTANCE OF COMMER-CIALLY PURE TITANIUM BY USING PLASMA NITROCARBURIZING PROCESS.* ACTA METALLURGICA SLOVACA, 2022. **28**(1): p. 14-18.
52. Istanbullu, O.B. and G. Akdogan, *Increased body fluid repellency and electrochemical corrosion resistance of intravascular stent materials by ICP-CVD-based DLC thin-film deposition.* Diamond and Related Materials, 2023. **138**: p. 110251.
53. Khodayari, A., et al., *Modified diamond-like carbon (Cr-DLC) coating applied by PACVD-CAPVD hybrid method: Characterization and evaluation of tribological and corrosion behavior.* Diamond and Related Materials, 2023. **136**: p. 109968.